Inorganic Chemistry

pubs.acs.org/IC

Article

Chelating Rare-Earth Metals (Ln^{3+}) and $^{225}Ac^{3+}$ with the Dual-Size-Selective Macrocyclic Ligand Py_2-Macrodipa

Aohan Hu, Megan E. Simms, Vilmos Kertesz, Justin J. Wilson,* and Nikki A. Thiele*

Cite This: *Inorg. Chem.* 2022, 61, 12847−12855

Read Online

ACCESS | Metrics & More | Article Recommendations | Supporting Information

ABSTRACT: Radioisotopes of metallic elements, or radiometals, are widely employed in both therapeutic and diagnostic nuclear medicine. For this application, chelators that efficiently bind the radiometal of interest and form a stable metal−ligand complex with it are required. Toward the development of new chelators for nuclear medicine, we recently reported a novel class of 18-membered macrocyclic chelators that is characterized by their ability to form stable complexes with both large and small rare-earth metals (Ln^{3+}), a property referred to as dual size selectivity. A specific chelator in this class called py-macrodipa, which contains one pyridyl group within its macrocyclic core, was established as a promising candidate for $^{135}La^{3+}$, $^{213}Bi^{3+}$, and $^{44}Sc^{3+}$ chelation. Building upon this prior work, here we report the synthesis and characterization of a new chelator called py_2-macrodipa with two pyridyl units fused into the macrocyclic backbone. Its coordination chemistry with the Ln^{3+} series was investigated by NMR spectroscopy, X-ray crystallography, density functional theory (DFT) calculations, analytical titrations, and transchelation assays. These studies reveal that py_2-macrodipa retains the expected dual size selectivity and possesses an enhanced thermodynamic affinity for all Ln^{3+} compared to py-macrodipa. By contrast, the kinetic stability of Ln^{3+} complexes with py_2-macrodipa is only improved for the light, large Ln^{3+} ions. Based upon these observations, we further assessed the suitability of py_2-macrodipa for use with $^{225}Ac^{3+}$, a large radiometal with valuable properties for targeted α therapy. Radiolabeling and stability studies revealed py_2-macrodipa to efficiently incorporate $^{225}Ac^{3+}$ and to form a complex that is inert in human serum over 3 weeks. Although py_2-macrodipa does not surpass the state-of-the-art chelator macropa for $^{225}Ac^{3+}$ chelation, it does provide another effective $^{225}Ac^{3+}$ chelator. These studies shed light on the fundamental coordination chemistry of the Ln^{3+} series and may inspire future chelator design efforts.

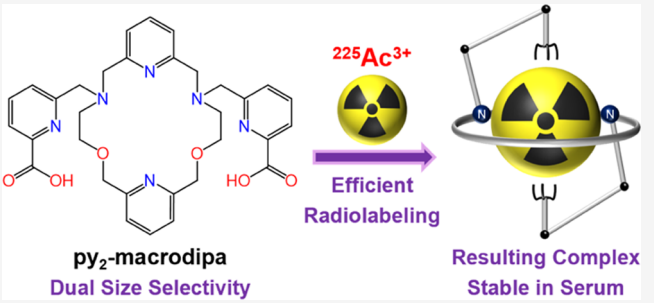

INTRODUCTION

Radiopharmaceutical agents, which leverage radionuclides for medicinal therapy and diagnosis, have been receiving increasing attention as new modalities progress to the clinic.[1−5] Across the entire periodic table, many metallic elements have been identified to possess radioisotopes suitable for this application.[6−8] To harness these radiometals for clinical use, a chelator that can rapidly form thermodynamically and kinetically stable complexes is usually required. Facile complex formation minimizes radioactivity loss during handling before in vivo administration, and high complex stability prevents in vivo release of the potentially harmful radiometal. A significant body of research has been devoted to chelator design for radiometals by addressing their distinct chemical properties and coordination chemistry preferences.[7−10]

As a recent contribution to this area, we developed a class of ligands that exhibit "dual size selectivity", a property characterized by their ability to preferentially bind both the large and small rare-earth metal (Ln^{3+}) ions. This dual-size-selective property is attributed to a significant conformational toggle that occurs in this ligand class as they bind metal ions of different sizes (Scheme 1) to optimize complex stability. For large Ln^{3+}, a 10-coordinate, nearly C_2-symmetric complex is formed (Conformation A), whereas for small Ln^{3+}, an 8-coordinate asymmetric complex arises (Conformation B).[10−12] The first identified member of this ligand class was the macrocyclic chelator macrodipa (Chart 1).[11] Despite the unique selectivity profile of macrodipa, the kinetic lability of the corresponding Ln^{3+}−macrodipa complexes limited its use for biomedical applications.[12]

To overcome this limitation, we modified the structure of macrodipa by incorporating a stronger pyridyl donor in place of an ethereal oxygen within the macrocycle to afford the second-generation ligand py-macrodipa (Chart 1). This change led to a significant enhancement of both the thermodynamic and kinetic stability of its Ln^{3+} complexes while maintaining its

Received: June 9, 2022
Published: August 1, 2022

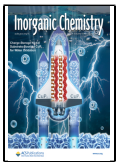

https://doi.org/10.1021/acs.inorgchem.2c01998
Inorg. Chem. 2022, 61, 12847−12855

Scheme 1. Depiction of the Conformational Toggle Present in Dual-Size-Selective Chelators when Binding Ln^{3+} Ions of Different Sizes[a]

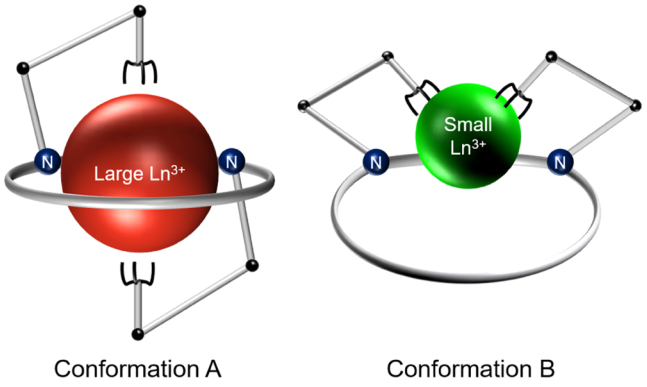

[a]Reproduced from *J. Am. Chem. Soc.* **2020**, *142*, 13500. Copyright 2020 American Chemical Society.

dual size selectivity. Based on these improvements of macrodipa, we showed that py-macrodipa efficiently formed stable complexes with $^{135}La^{3+}$ and $^{44}Sc^{3+}$, two valuable radionuclides for nuclear medicine with significantly disparate ionic radii.[12] To further validate the potential of py-macrodipa for nuclear medicine applications, we assessed its suitability for chelating $^{225}Ac^{3+}$ and $^{213}Bi^{3+}$, two therapeutically valuable α-emitters.[13,14] These studies showed that py-macrodipa is a promising candidate for $^{213}Bi^{3+}$ chelation but does not form a complex of sufficient kinetic stability for $^{225}Ac^{3+}$ nuclear medicine applications.[15]

The inefficacy of py-macrodipa for the stable chelation of $^{225}Ac^{3+}$ motivated us to target a third-generation dual-size-selective chelator that forms complexes with even greater thermodynamic and kinetic stability. Based on the improvements that were observed upon the incorporation of a single pyridyl group into the macrocycle of macrodipa, we targeted the novel chelator py_2-macrodipa (Chart 1), which contains an additional pyridyl donor. In this work, we discuss the synthesis of this new ligand, its coordination chemistry with Ln^{3+} ions, and its potential application for $^{225}Ac^{3+}$ radiotherapy.

RESULTS AND DISCUSSION

The chelator py_2-macrodipa was synthesized via the five-step procedure shown in Scheme 2, with an overall yield of 20%. The benzyl-protected macrocyclic backbone **2** was constructed in two steps commencing from commercially available 2,6-bis(bromomethyl)pyridine and 2-benzylaminoethanol. The benzyl groups were then removed by reduction with H_2 over a Pd/C catalyst to yield the desired dipyridyl macrocycle **3**. Subsequent installation of the two picolinate pendent arms via alkylation and acidic deprotection afforded py_2-macrodipa. The identity and purity of the intermediates and final products were verified by NMR spectroscopy, mass spectrometry, and analytical high-performance liquid chromatography (HPLC) (Figures S1−S13).

To understand the influence of the second pyridyl unit on the coordination chemistry of py_2-macrodipa, the crystal structures of its complexes with two representative Ln^{3+} ions, La^{3+} and Sc^{3+}, were determined by X-ray crystallography (Figure 1). La^{3+}, the largest Ln^{3+}, forms a complex with py_2-macrodipa that attains the 10-coordinate, distorted C_2-symmetric Conformation A, with all nitrogen and oxygen donor atoms on the ligand engaged in metal binding. By contrast, the py_2-macrodipa complex of Sc^{3+}, the smallest Ln^{3+}, adopts the 8-coordinate, asymmetric Conformation B. In this crystal structure, three of the macrocycle-based ligand donor atoms (O1, O2, N4) do not directly interact with the Sc^{3+} center, whose coordination sphere is completed by an inner-sphere water molecule. The conformations observed for the La^{3+} and Sc^{3+} crystal structures are in line with our expectations, based on the well-characterized conformational toggle (Scheme 1) observed for the earlier generation analogues, macrodipa and py-macrodipa, upon binding to Ln^{3+} of different sizes.[11,12]

Having verified that this conformational change occurs in the solid state, we next leveraged NMR spectroscopy to characterize the solution structures of Ln^{3+}−py_2-macrodipa complexes with the diamagnetic La^{3+}, Y^{3+}, Lu^{3+}, and Sc^{3+} ions, for which the ionic radius decreases from 103.2 to 74.5 pm.[16] The ^1H and $^{13}C\{^1H\}$ NMR spectra of these four complexes were acquired in D_2O at pD 7 (Figures 2 and S17−S24). Figure 2 shows a stacked arrangement of the ^1H NMR spectra

Chart 1. Structures of Ligands Discussed in this Work

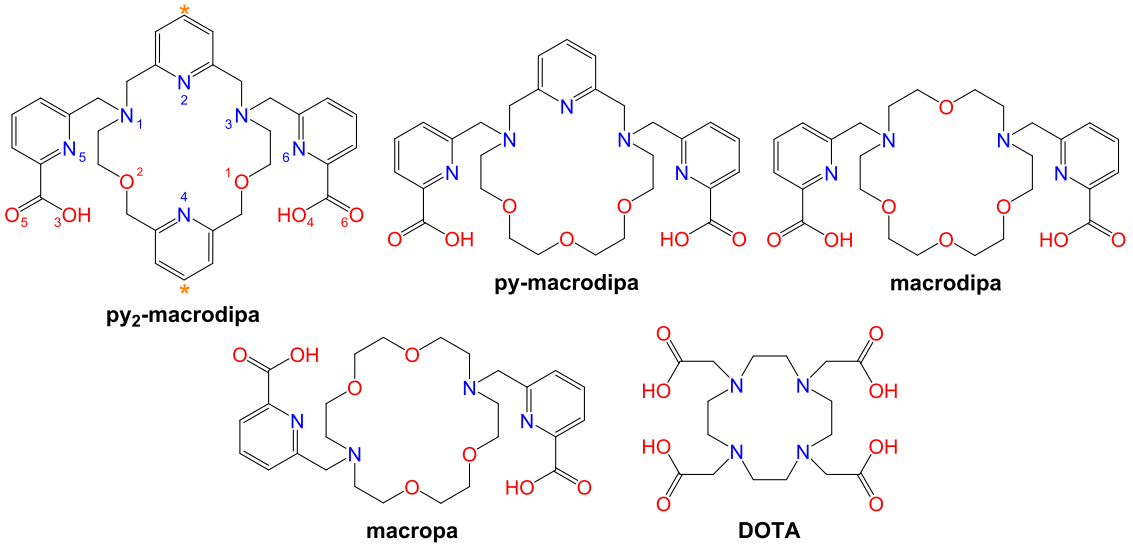

https://doi.org/10.1021/acs.inorgchem.2c01998
Inorg. Chem. 2022, 61, 12847−12855

Scheme 2. Synthetic Route to Py_2-Macrodipa

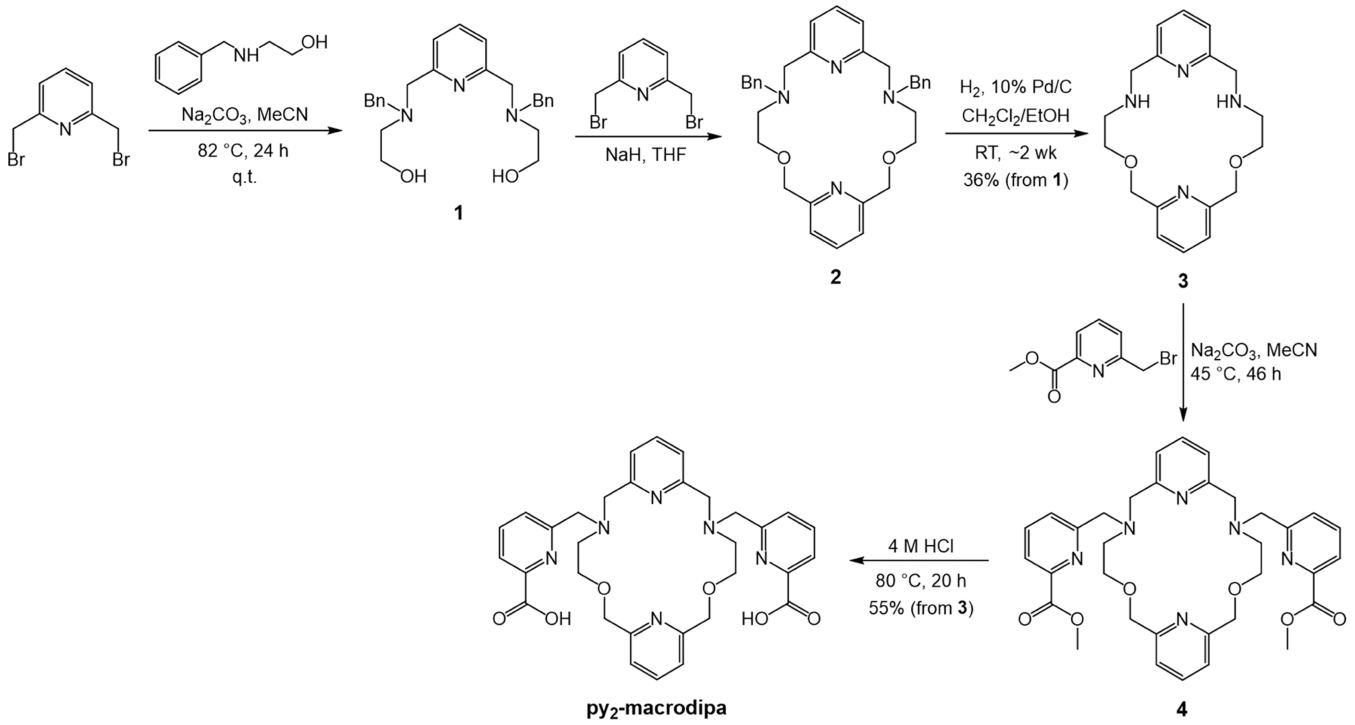

of these four complexes for comparison. The ^{1}H NMR spectra of the complexes of La^{3+} and Y^{3+} show equivalency in their resonances, indicating that the symmetric Conformation A predominates for the py_2-macrodipa complexes of these larger ions. By contrast, Sc^{3+}, the smallest Ln^{3+}, yields an NMR spectrum of lower symmetry, revealing it to attain the asymmetric Conformation B in aqueous solution. The $^{13}C\{^1H\}$ NMR spectra of these complexes are also consistent with these conformational assignments (Figures S18, S20, and S24). These NMR observations indicate that the solid-state crystallographic studies of the La^{3+} and Sc^{3+} complexes (Figure 1) are a good representation of their solution structures.

The ^{1}H NMR spectrum of the py_2-macrodipa complex of the intermediately-sized Lu^{3+} is more complicated than those of La^{3+}, Y^{3+}, and Sc^{3+}. Two different species, in a molar ratio of 4:1, are observed. The $^{13}C\{^1H\}$ NMR spectrum of this complex likewise reveals the presence of two species (Figure S22). These two species are assigned to be a mixture of Conformations A and B in equilibrium. A close inspection of the aromatic region of the ^{1}H NMR spectrum (Figures 2 and S21) reveals an asymmetry in both conformers, despite our prior observations that Conformation A typically gives rise to spectra with symmetry. Our tentative explanation for this observation is that the Conformation A gradually descends in symmetry as the Ln^{3+} gets smaller, and the size-matching becomes poorer. This argument is supported by comparing the ^{1}H NMR spectra of the large La^{3+} and smaller Y^{3+} complexes (Figure 2), where a decrease in the symmetry of Conformation A begins to appear. Most apparent are the two triplets in the aromatic region (labeled with orange asterisks), which can be assigned to the geminal hydrogens on the carbon atoms labeled with orange asterisks in Chart 1. For the large La^{3+}, the chemical shifts of these two triplets are nearly identical, whereas for the smaller Y^{3+}, their chemical shifts begin to diverge more substantially and indicate different chemical environments for these two H atoms, presumably due to a decrease in the symmetry of Conformation A.

To further understand the conformational switch of py_2-macrodipa across the Ln^{3+} series, we carried out density functional theory (DFT) calculations. All Ln^{3+}–py_2-macrodipa complexes in both Conformations A and B were optimized, using the same level of theory (ωB97XD/6-31G(d,p)/LCRECP) that we previously applied to study Ln^{3+}–macrodipa and Ln^{3+}–py-macrodipa complexes.[11,12,17−24] From these geometry optimizations and thermochemical calculations, the standard free-energy difference ($\Delta G°$) between Conformations A and B for each Ln^{3+} complex was determined (eq 1), as plotted in Figure 3.

$$[Ln(py_2\text{-macrodipa})]^+(\text{Conformation A}, aq) + H_2O(l) \rightleftharpoons [Ln(py_2\text{-macrodipa})(OH_2)]^+(\text{Conformation B}, aq) \quad (1)$$

As the Ln^{3+} series is traversed, $\Delta G°$ gradually shifts from positive to negative values, consistent with our experimental observations that Conformation A is favored for large Ln^{3+}, whereas Conformation B is preferred for small Ln^{3+}. A similar computational analysis was applied in our studies with macrodipa and py-macrodipa, which also showed that Conformation A was lower in free energy for large Ln^{3+} and vice versa. The crossover point where $\Delta G°$ switches its sign occurs roughly at Tm^{3+}, Er^{3+}, and Tb^{3+} for py_2-macrodipa, py-macrodipa,[12] and macrodipa[11] systems, respectively. Thus, modifications of the macrocycle can alter the conformational dynamics and preferences of this ligand class.

Having confirmed by X-ray crystallography and NMR spectroscopy that Ln^{3+} complexes of py_2-macrodipa undergo a Ln^{3+} size-dependent conformational toggle like its earlier analogues macrodipa and py-macrodipa, we next set out to verify our hypothesis that the additional macrocyclic pyridyl moiety would lead to enhanced complex stability. In this

https://doi.org/10.1021/acs.inorgchem.2c01998
Inorg. Chem. 2022, 61, 12847−12855

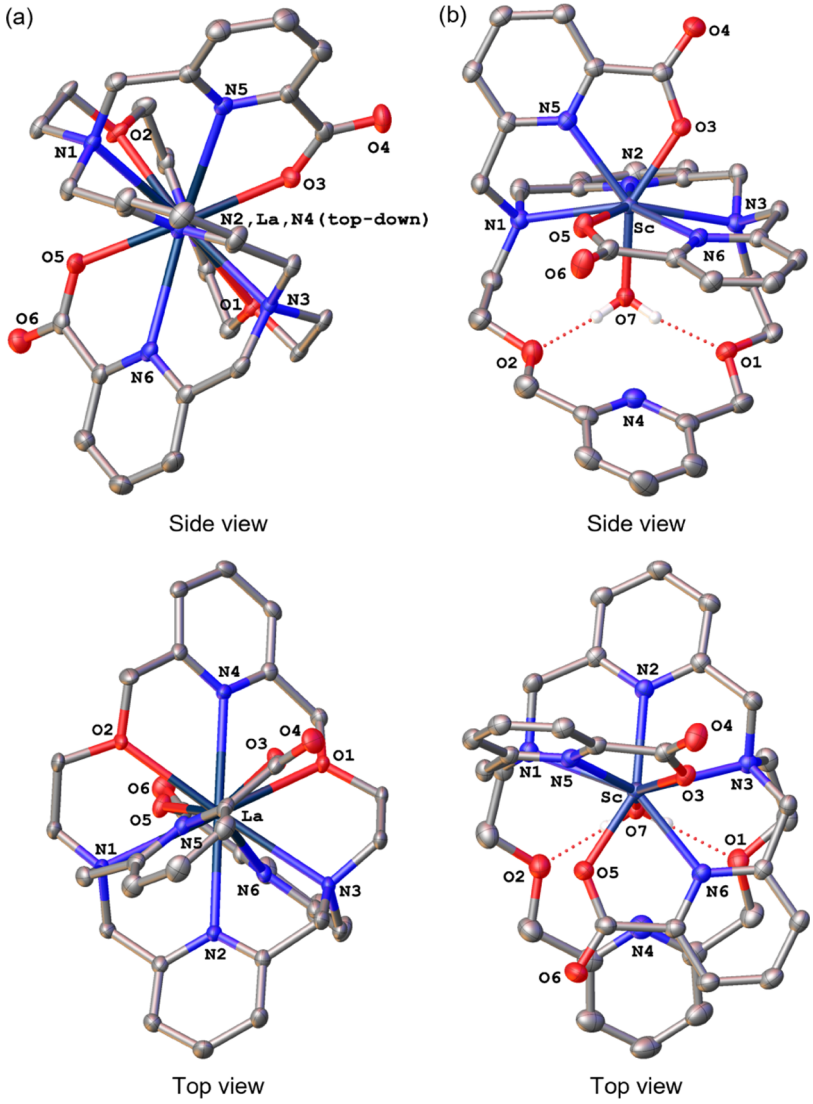

Figure 1. Crystal structures of (a) $[La(py_2\text{-macrodipa})]^+$ and (b) $[Sc(py_2\text{-macrodipa})(OH_2)]^+$. Thermal ellipsoids are drawn at the 50% probability level. Solvent, counterions, and nonacidic hydrogen atoms are omitted for clarity.

regard, we first evaluated the thermodynamic stability of Ln^{3+}–py_2-macrodipa complexes by determining their stability constants. The magnitude of the stability constant measures the thermodynamic affinity of a ligand for a metal ion and is valuable for assessing its potential in different applications.[10,25,26] The protonation constants (K_i) of py_2-macrodipa, as well as the stability constants (K_{LnL}) of its Ln^{3+} complexes, measured via either potentiometric titrations or ultraviolet–visible (UV–Vis) spectrophotometric titrations,[27−29] are collected in Table 1. These quantities are defined in eqs 2 and 3, where the concentration terms represent those at chemical equilibrium and L signifies the uncomplexed ligand in its fully deprotonated state.

$$K_i = [H_iL]/[H^+][H_{i-1}L] \quad (2)$$

$$K_{LnL} = [LnL]/[Ln^{3+}][L] \quad (3)$$

The log K_{LnL} values of py_2-macrodipa, and those of the related structures macrodipa, py-macrodipa, and macropa, are plotted against the Ln^{3+} 6-coordinate ionic radius[16] in Figure 4. Like macrodipa and py-macrodipa, py_2-macrodipa exhibits a dual-size-selective pattern that is not altered via the introduction of an additional pyridyl group in the macrocycle. Importantly, the log K_{LnL} values of py_2-macrodipa are systematically greater compared to those of py-macrodipa, indicating that the additional macrocyclic pyridyl group of py_2-macrodipa has a pronounced effect on enhancing the overall Ln^{3+} binding affinity. The log K_{LnL} values of py_2-macrodipa are also significantly higher across the entire Ln^{3+} series than those of macropa, a chelator established as a promising candidate for several large radiometals including $^{225}Ac^{3+}$, $^{132/135}La^{3+}$, $^{131}Ba^{2+}$, $^{223}Ra^{2+}$, and $^{213}Bi^{3+}$.[30−34] This observation highlights the potential of py_2-macrodipa for large radiometal chelation. Although these log K_{LnL} values are smaller than those observed for the Ln^{3+} complexes of the commonly applied chelator DOTA[35] (Chart 1), for which log K_{LnL} spans 22.9–25.4 from La^{3+} to Lu^{3+},[36] the established efficacy of macropa, which gives rise to substantially lower log K_{LnL} values for these radiometals, demonstrates that such high K_{LnL} values are not strictly needed for practical use in nuclear medicine. However, future ligand design efforts within this ligand class to increase these stability constants may further improve value for use in nuclear medicine.

https://doi.org/10.1021/acs.inorgchem.2c01998
Inorg. Chem. 2022, 61, 12847−12855

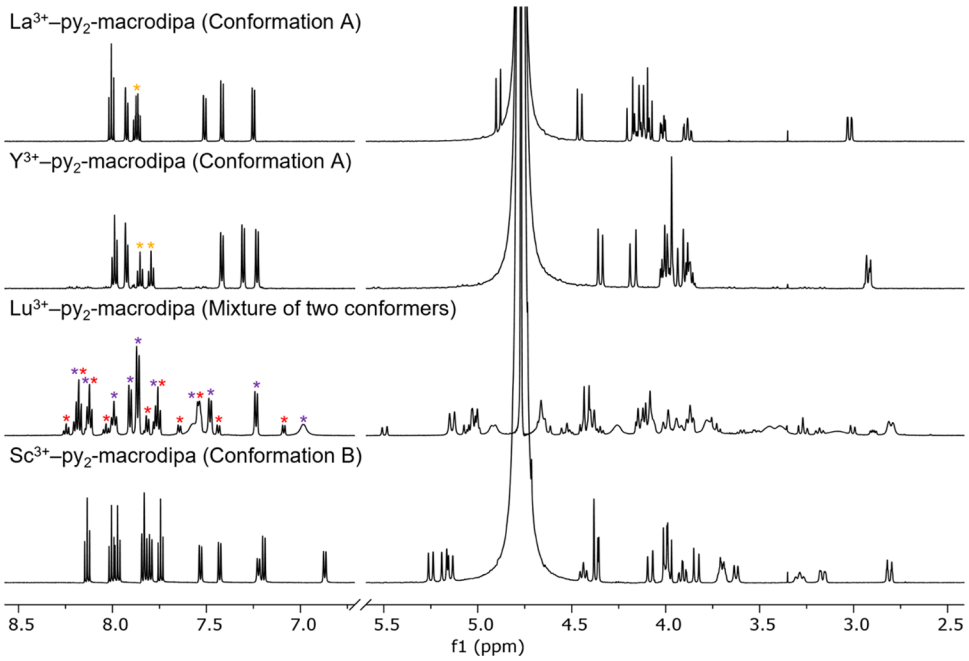

Figure 2. ^{1}H NMR spectra of La^{3+}–, Y^{3+}–, Lu^{3+}–, and Sc^{3+}–py_2-macrodipa complexes (600 MHz, D_2O, pD 7, 25 °C). The orange asterisks in the spectra of the La^{3+} and Y^{3+} complexes highlight the decrease in symmetry of Conformation A in moving from larger to smaller ions. The purple and red asterisks in the spectrum of the Lu^{3+} complex indicate the two conformers present in solution.

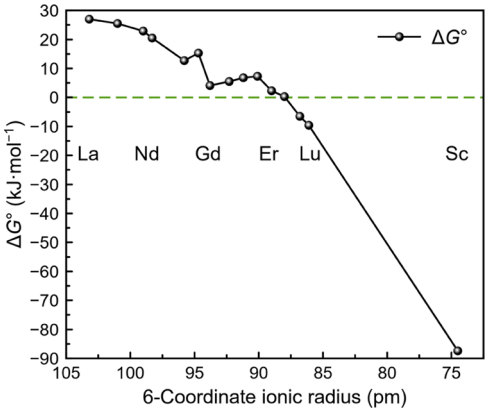

Figure 3. DFT-computed standard free-energy differences ($\Delta G°$) between Conformations A and B for Ln^{3+}–py_2-macrodipa complexes, plotted versus ionic radii.

Notably, the increase in $\log K_{LnL}$ in moving from py-macrodipa to py_2-macrodipa is much greater for the large Ln^{3+} than for the small Ln^{3+}. This observation can be rationalized by the crystal structures. The newly introduced second pyridyl unit directly interacts and stabilizes the metal center in Conformation A (Figure 1a), whereas it is not bound to the metal in Conformation B (Figure 1b). As such, Conformation A benefits more significantly from the presence of the additional macrocyclic pyridyl donor present in py_2-macrodipa. Thus, for large Ln^{3+} complexes, for which Conformation A prevails, a substantial $\log K_{LnL}$ enhancement is observed, but a diminished impact is found for small Ln^{3+} complexes, where Conformation B is dominant. Another noteworthy characteristic discerned from our potentiometric titrations is the identification of the protonated complex species (LnHL) for late Ln^{3+}–py_2-macrodipa systems (Figures S30–S34), which was not observed for any Ln^{3+}–py-macrodipa complexes.[12] Based on this information, the most likely protonation site to form the LnHL species is the second pyridyl group (N4, Chart 1), which is substantially basic and not directly engaged with the Ln^{3+} center (Figure 1b) in Conformation B.

Table 1. Protonation Constants of and Ln^{3+} Stability Constants of Py_2-Macrodipa, Py-Macrodipa, Macrodipa, and Macropa

	py_2-macrodipa[a]	py-macrodipa	macrodipa	macropa
$\log K_1$	7.58(4)	7.20[b]	7.79[c]	7.41[d], 7.41[e]
$\log K_2$	6.48(1)	6.54[b]	7.04[c]	6.85[d], 6.90[e]
$\log K_3$	3.52(3)	3.17[b]	3.18[c]	3.32[d], 3.23[e]
$\log K_4$	2.60(5)	2.31[b]	2.41[c]	2.36[d], 2.45[e]
$\log K_5$	2.10(11)			1.69[d]
$\log K_{LaL}$	16.68(8)	14.31[b]	12.19[c]	14.99[d]
$\log K_{CeL}$	17.13(7)	14.65[b]	12.50[c]	15.11[d]
$\log K_{PrL}$	17.28(6)	14.81[b]	12.41[c]	14.70[d]
$\log K_{NdL}$	17.11(3)	14.51[b]	12.25[c]	14.36[d]
$\log K_{SmL}$	16.56(4)	13.66[b]	11.52[c]	13.80[d]
$\log K_{EuL}$	15.93(4)	13.29[b]	10.93[c]	13.01[d]
$\log K_{GdL}$	15.25(7)	12.63[b]	10.23[c]	13.02[d]
$\log K_{TbL}$	14.76(6)	11.95[b]	9.68[c]	11.79[d]
$\log K_{DyL}$	14.04(2)	11.47[b]	9.36[c]	11.72[d]
$\log K_{HoL}$	12.68(5)	10.69[b]	9.36[c]	10.59[d]
$\log K_{ErL}$	12.17(3)	10.60[b]	9.71[c]	10.10[d]
$\log K_{TmL}$	11.98(2)	10.92[b]	10.13[c]	9.59[d]
$\log K_{YbL}$	11.82(5)	11.31[b]	10.48[c]	8.89[d]
$\log K_{LuL}$	11.90(3)	11.54[b]	10.64[c]	8.25[d]
$\log K_{ScL}$	16.28(4)	15.83[b]	14.37[b]	

[a]0.1 M KCl, this work. The values in the parentheses are one standard deviation of the last significant figure. [b]0.1 M KCl, ref 12. [c]0.1 M KCl, ref 11. [d]0.1 M KCl, ref 37. [e]0.1 M KCl, ref 38.

After demonstrating an enhancement of Ln^{3+} complex thermodynamic stability afforded by the second pyridyl group of py_2-macrodipa, we next evaluated its impact on complex kinetic stability, a property of critical importance for chelators

https://doi.org/10.1021/acs.inorgchem.2c01998
Inorg. Chem. 2022, 61, 12847−12855

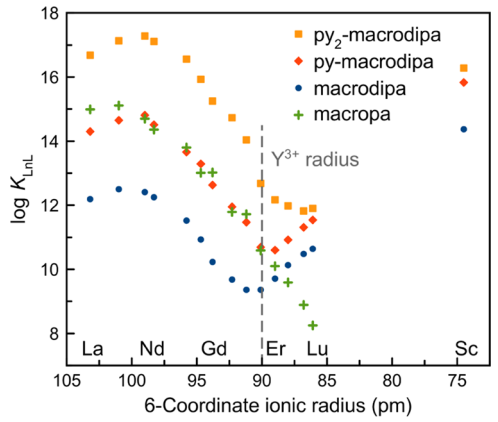

Figure 4. Stability constants of Ln^{3+} complexes formed with py_2-macrodipa, py-macrodipa, macrodipa, and macropa plotted versus ionic radii.

applied in radiopharmaceutical settings.[1,9] For comparison to our previous studies, an identical DTPA transchelation challenge[12,39] was applied to assess the Ln^{3+}–py_2-macrodipa complex kinetic stability. Specifically, the complexes were treated with 100 equiv of DTPA at pH 7.4 and room temperature (RT, 22 °C), a condition that thermodynamically favors the formation of the Ln^{3+}–DTPA complexes.[40−42] This transchelation process, which follows pseudo-first-order kinetics with the large excess of DTPA, was monitored by UV–Vis spectroscopy. The half-lives ($t_{1/2}$) afforded from these pseudo-first-order processes (Table 2) provide a quantitative comparative measure of the complex kinetic stability.

Table 2. Half-Lives of Ln^{3+}–Py_2-Macrodipa, Ln^{3+}–Py-Macrodipa, and Ln^{3+}–Macrodipa Complexes when Challenged with 100 Equivalents of DTPA[a]

	Ln^{3+}–py_2-macrodipa	Ln^{3+}–py-macrodipa[b]	Ln^{3+}–macrodipa[b]
La^{3+}	≫5 weeks	6.3 d	1678 s
Gd^{3+}	4.5 ± 0.2 d	5524 s	54 s
Lu^{3+}	253 ± 6 s	853 s	65 s
Sc^{3+}	5.9 ± 0.4 h	16.6 h	782 s

[a][LnL] = 100 μM, pH 7.4 in MOPS, 22 °C. [b]Ref 12.

The trend in kinetic stability of the Ln^{3+}–py_2-macrodipa complexes follows closely with that observed for their thermodynamic stability, with the light and heavy Ln^{3+} complexes undergoing slower transchelation than those in the middle of the series. In comparison to those of macrodipa and py-macrodipa, the early Ln^{3+} complexes of py_2-macrodipa exhibit a remarkable kinetic stability, with <10% dissociation of the La^{3+} complex observed after 5 weeks (Figure S41). However, for the smallest Sc^{3+}, the kinetic stability of its py_2-macrodipa complex is significantly lower than that of py-macrodipa, indicating that the second macrocyclic pyridyl is detrimental in this regard. The enhancement of kinetic stability of the La^{3+} complex is easily rationalized from the X-ray crystallographic data (Figure 1a), where both pyridyl groups strongly engage the La^{3+} center. By contrast, the non-coordinated pyridyl group present in the Sc^{3+}–py_2-macrodipa complex is positioned closely to the inner-sphere water molecule (Figure 1b N4–O7 distance of 2.91 Å), within a range that is consistent with hydrogen bonding, for which the N···O distances typically span from 2.8 to 3.0 Å.[43] Thus, the pendent pyridyl group is oriented appropriately to facilitate proton-assisted metal ion dissociation, which substantially labilizes the complex in aqueous solution. The increasing kinetic lability by protonation was also illustrated in other metal complex systems.[44−46] Collectively, the inclusion of this second pyridyl unit of py_2-macrodipa enhances the thermodynamic stability for all Ln^{3+} complexes but only improves the kinetic stability of complexes with the large Ln^{3+}. Thus, py_2-macrodipa is a promising candidate for large Ln^{3+} chelation.

On account of the remarkable thermodynamic and kinetic stability of the La^{3+}–py_2-macrodipa complex, we next sought to investigate the ability of py_2-macrodipa to chelate the largest trivalent cation Ac^{3+}, as both ions possess similar coordination chemistry.[47] Furthermore, the radioisotope $^{225}Ac^{3+}$ ($t_{1/2}$ = 9.9 d)[48] emits four α particles through its decay chain, making it valuable for use in targeted internal radiotherapy.[49−51] To assess the suitability of py_2-macrodipa as a chelator for this radiometal, we carried out $^{225}Ac^{3+}$ radiolabeling studies with py_2-macrodipa and benchmarked the results to macropa and DOTA (Chart 1), two macrocyclic chelators that have established precedence for $^{225}Ac^{3+}$ chelation.[30,52]

Concentration-dependent radiolabeling studies were carried out by incubating different concentrations of py_2-macrodipa, macropa, and DOTA with 9.5–11.1 kBq of $^{225}Ac^{3+}$ at pH 6.0 and 25 °C. The radiochemical yields (RCYs), determined by radio-thin layer chromatography (radio-TLC), are summarized in Figure 5 and Table S3. Notably, py_2-macrodipa quantitatively incorporates $^{225}Ac^{3+}$ at a low concentration of 10^{-5} M within 5 min, revealing it to be an efficient chelator for

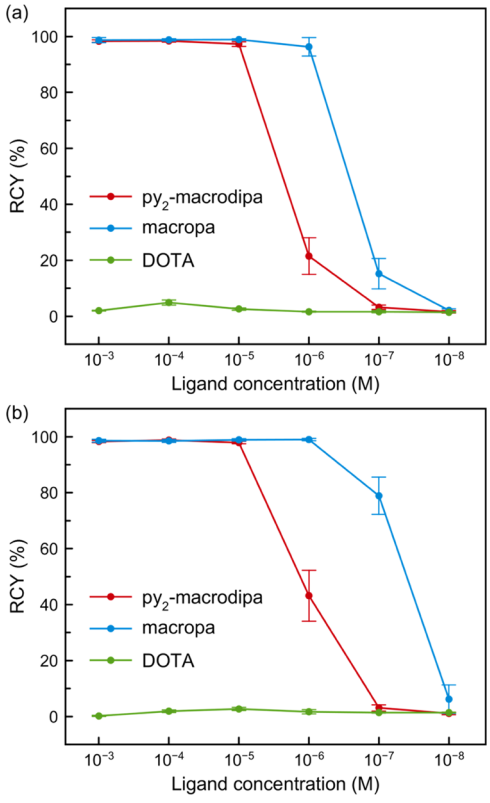

Figure 5. Radiochemical yields (RCYs) of $^{225}Ac^{3+}$ radiolabeling with py_2-macrodipa, macropa, and DOTA at different ligand concentrations (pH 6.0, 25 °C): (a) 5 min reaction time and (b) 60 min reaction time.

https://doi.org/10.1021/acs.inorgchem.2c01998
Inorg. Chem. 2022, 61, 12847−12855

$^{225}Ac^{3+}$. This property is nearly on par with that of macropa, the current gold standard, which quantitatively radiolabels $^{225}Ac^{3+}$ at micromolar concentration, an observation consistent with previously reported results.[15,30] By contrast, DOTA did not significantly undergo $^{225}Ac^{3+}$ radiolabeling even at a millimolar concentration. Increasing the reaction time to 60 min had only a slight effect on the RCYs for py_2-macrodipa and macropa, indicating that the radiolabeling process is nearly complete within 5 min under these mild conditions for both chelators. In addition, the radiolabeling efficiency of py_2-macrodipa is comparable to that of py-macrodipa and significantly better than macrodipa.[15]

After establishing effective radiolabeling of py_2-macrodipa with $^{225}Ac^{3+}$, the kinetic stability of its $^{225}Ac^{3+}$ complex was assessed. Specifically, the $^{225}Ac^{3+}$ complexes of py_2-macrodipa and macropa were incubated in human serum at 37 °C over 3 weeks to model the conditions that would be encountered when a radiopharmaceutical agent is administered in vivo. Figure 6 shows the percentage of intact complex remaining

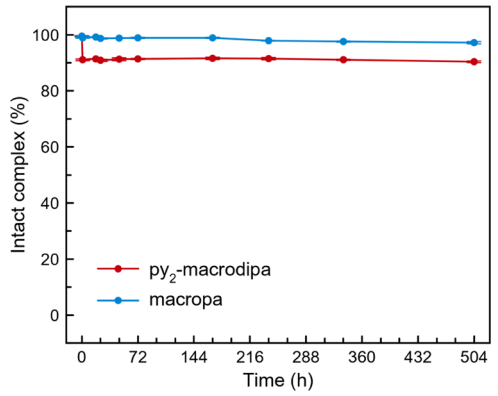

Figure 6. Stability of $[^{225}Ac]Ac^{3+}$–py_2-macrodipa and $[^{225}Ac]Ac^{3+}$–macropa in human serum at 37 °C.

throughout the course of this experiment. Both radiocomplexes are sufficiently stable in human serum, as reflected by the fact that they remain >90% intact after 3 weeks. The resistance to human serum for $[^{225}Ac]Ac^{3+}$–macropa observed here is also consistent with prior studies.[15,30,53] Although the radiolabeling efficiency of py_2-macrodipa is comparable to that of py-macrodipa, the kinetic stability of $[^{225}Ac]Ac^{3+}$–py_2-macrodipa is substantially enhanced relative to that of $[^{225}Ac]Ac^{3+}$–py-macrodipa, which showed a ∼90% complex dissociation in human serum at 37 °C after 24 h.[15] This observation is also consistent with the DTPA transchelation challenge results (Table 2), which also revealed an overall higher Ln^{3+} complex kinetic stability for py_2-macrodipa. Collectively, py_2-macrodipa shows promise for use with $^{225}Ac^{3+}$ based on its efficient radiolabeling and high complex stability. It exhibits the best performance for $^{225}Ac^{3+}$ chelation among the dual-size-selective chelators.

CONCLUSION

Building upon macrodipa and py-macrodipa, we designed and prepared the third-generation dual-size-selective chelator py_2-macrodipa. Its coordination chemistry with Ln^{3+} ions was characterized by multiple techniques including X-ray crystallography, NMR spectroscopy, DFT calculations, analytical titrations, and transchelation assays. These three chelators all exhibit dual-size-selective properties and are based on the same 18-membered macrocyclic core structures. They differ in the presence of 0, 1, or 2 pyridyl groups within the macrocyclic core. Without an integrated pyridyl group, macrodipa is a relatively poor chelator with respect to both the thermodynamic and kinetic stability of its Ln^{3+} complexes. The single pyridyl group in py-macrodipa serves to enhance both properties. In this study, we showed that the introduction of a second pyridyl group in py_2-macrodipa further enhanced the thermodynamic stability for all Ln^{3+} complexes, but the kinetic stability was only improved for the large Ln^{3+} complexes. As a general conclusion, it appears that the inclusion of pyridyl groups in place of ethereal donors does benefit complex stability, but the conformations of the resulting complexes also need to be considered when trying to anticipate the magnitudes of these effects. Despite the weaker performance of py_2-macrodipa for small Ln^{3+}, its promising chelation properties for large Ln^{3+} prompted us to investigate its use with the therapeutic radiometal $^{225}Ac^{3+}$. Radiolabeling and serum stability studies with $^{225}Ac^{3+}$ revealed py_2-macrodipa to perform comparably to the state-of-the-art chelator macropa. Although the dual-size-selective properties were demonstrated both thermodynamically and kinetically, efforts need to be undertaken to improve the stability of its complexes with small metal ions for practical nuclear medicine applications. Additionally, ongoing work is also directed toward preparation of a bifunctional analogue of py_2-macrodipa that can be used to conjugate with biomolecules. Both the macrocyclic backbone and the picolinate pendent arms provide potential opportunities for this functionalization. In any case, this work affords a new potential candidate for $^{225}Ac^{3+}$ chelation as well as provides new insights on the fundamental Ln^{3+} coordination chemistry and $^{225}Ac^{3+}$ radiochemistry for future chelator development endeavors.

ASSOCIATED CONTENT

Supporting Information

The Supporting Information is available free of charge at https://pubs.acs.org/doi/10.1021/acs.inorgchem.2c01998.

Experimental procedures and supplementary data for ligand synthesis, X-ray crystallography, NMR spectroscopy, DFT calculations, potentiometric titrations, UV–vis spectrophotometric titrations; DTPA transchelation studies, radiolabeling studies, and serum challenge assays (PDF)

Geometry outputs for all DFT-optimized structures (ZIP)

Accession Codes

CCDC 2178140–2178141 contain the supplementary crystallographic data for this paper. These data can be obtained free of charge via www.ccdc.cam.ac.uk/data_request/cif, or by emailing data_request@ccdc.cam.ac.uk, or by contacting The Cambridge Crystallographic Data Centre, 12 Union Road, Cambridge CB2 1EZ, UK; fax: +44 1223 336033.

AUTHOR INFORMATION

Corresponding Authors

Justin J. Wilson − *Department of Chemistry and Chemical Biology, Cornell University, Ithaca, New York 14853, United States;* orcid.org/0000-0002-4086-7982; Email: jjw275@cornell.edu.

Nikki A. Thiele − *Chemical Sciences Division, Oak Ridge National Laboratory, Oak Ridge, Tennessee 37830, United*

https://doi.org/10.1021/acs.inorgchem.2c01998
Inorg. Chem. 2022, 61, 12847−12855

States; orcid.org/0000-0003-3301-0849;
Email: thielena@ornl.gov

Authors

Aohan Hu − *Department of Chemistry and Chemical Biology, Cornell University, Ithaca, New York 14853, United States;* orcid.org/0000-0002-9720-3159

Megan E. Simms − *Chemical Sciences Division, Oak Ridge National Laboratory, Oak Ridge, Tennessee 37830, United States*

Vilmos Kertesz − *Biosciences Division, Oak Ridge National Laboratory, Oak Ridge, Tennessee 37830, United States;* orcid.org/0000-0003-0186-5797

Complete contact information is available at: https://pubs.acs.org/10.1021/acs.inorgchem.2c01998

Notes

The authors declare the following competing financial interest(s): A.H, J.J.W., and N.A.T. are co-inventors on a patent application filed on the use of py2-macrodipa and related analogues for nuclear medicine applications.

■ ACKNOWLEDGMENTS

This research was supported by the Department of Energy Isotope Program, managed by the Office of Science for Isotope R&D and Production, and by the Laboratory Directed Research and Development Program of Oak Ridge National Laboratory (ORNL). The authors would like to thank the staff of the Technical Services, Finishing, and Dispensing Group at ORNL for their isotope production and purification contributions. The manuscript was produced by UT-Battelle, LLC under Contract No. DE-AC05-00OR22725 with the U.S. Department of Energy (DOE). The publisher acknowledges the Government license to provide public access under the DOE Public Access Plan (http://energy.gov/downloads/doe-public-access-plan). This research was also supported by the National Institutes of Biomedical Imaging and Bioengineering of the National Institutes of Health under Award Numbers R21EB027282 and R01EB029259, as well as by the DOE Office of Science under Award Number DE-SC0021662. J.J.W. thanks the Research Corporation for Science Advancement for a Cottrell Scholar Award. A.H. was funded by a summer research fellowship at ORNL via the ORISE/ORAU (GSO program) to work on this project. V.K. was supported by the DOE Office of Biological and Environmental Research. We thank Dr. Samantha MacMillan for data collection on the X-ray diffractometer.

■ REFERENCES

(1) *Radiopharmaceutical Chemistry*; Lewis, J. S.; Windhorst, A. D.; Zeglis, B. M., Eds.; Springer Nature Switzerland AG: Cham, Switzerland, 2019.

(2) Dondi, M.; Kashyap, R.; Paez, D.; Pascual, T.; Zaknun, J.; Bastos, F. M.; Pynda, Y. Trends in Nuclear Medicine in Developing Countries. *J. Nucl. Med.* **2011**, *52*, 16S−23S.

(3) Delbeke, D.; Segall, G. M. Status of and Trends in Nuclear Medicine in the United States. *J. Nucl. Med.* **2011**, *52*, 24S−28S.

(4) Kramer-Marek, G.; Capala, J. The Role of Nuclear Medicine in Modern Therapy of Cancer. *Tumor Biol.* **2012**, *33*, 629−640.

(5) Sgouros, G.; Bodei, L.; McDevitt, M. R.; Nedrow, J. R. Radiopharmaceutical Therapy in Cancer: Clinical Advances and Challenges. *Nat. Rev. Drug Discovery* **2020**, *19*, 589−608.

(6) Blower, P. J. A Nuclear Chocolate Box: the Periodic Table of Nuclear Medicine. *Dalton Trans.* **2015**, *44*, 4819−4844.

(7) Kostelnik, T. I.; Orvig, C. Radioactive Main Group and Rare Earth Metals for Imaging and Therapy. *Chem. Rev.* **2019**, *119*, 902−956.

(8) Boros, E.; Packard, A. B. Radioactive Transition Metals for Imaging and Therapy. *Chem. Rev.* **2019**, *119*, 870−901.

(9) Price, E. W.; Orvig, C. Matching Chelators to Radiometals for Radiopharmaceuticals. *Chem. Soc. Rev.* **2014**, *43*, 260−290.

(10) Hu, A.; Wilson, J. J. Advancing Chelation Strategies for Large Metal Ions for Nuclear Medicine Applications. *Acc. Chem. Res.* **2022**, *55*, 904−915.

(11) Hu, A.; MacMillan, S. N.; Wilson, J. J. Macrocyclic Ligands with an Unprecedented Size-Selectivity Pattern for the Lanthanide Ions. *J. Am. Chem. Soc.* **2020**, *142*, 13500−13506.

(12) Hu, A.; Aluicio-Sarduy, E.; Brown, V.; MacMillan, S. N.; Becker, K. V.; Barnhart, T. E.; Radchenko, V.; Ramogida, C. F.; Engle, J. W.; Wilson, J. J. Py-Macrodipa: A Janus Chelator Capable of Binding Medicinally Relevant Rare-Earth Radiometals of Disparate Sizes. *J. Am. Chem. Soc.* **2021**, *143*, 10429−10440.

(13) Morgenstern, A.; Apostolidis, C.; Kratochwil, C.; Sathekge, M.; Krolicki, L.; Bruchertseifer, F. An Overview of Targeted Alpha Therapy with ^{225}Actinium and ^{213}Bismuth. *Curr. Radiopharm.* **2018**, *11*, 200−208.

(14) Bruchertseifer, F.; Kellerbauer, A.; Malmbeck, R.; Morgenstern, A. Targeted Alpha Therapy with Bismuth-213 and Actinium-225: Meeting Future Demand. *J. Label. Compd. Radiopharm.* **2019**, *62*, 794−802.

(15) Hu, A.; Brown, V.; MacMillan, S. N.; Radchenko, V.; Yang, H.; Wharton, L.; Ramogida, C. F.; Wilson, J. J. Chelating the Alpha Therapy Radionuclides $^{225}Ac^{3+}$ and $^{213}Bi^{3+}$ with 18-Membered Macrocyclic Ligands Macrodipa and Py-Macrodipa. *Inorg. Chem.* **2022**, *61*, 801−806.

(16) Shannon, R. D. Revised Effective Ionic Radii and Systematic Studies of Interatomic Distances in Halides and Chalcogenides. *Acta Crystallogr., Sect. A* **1976**, *32*, 751−767.

(17) Frisch, M. J.; Trucks, G. W.; Schlegel, H. B.; Scuseria, G. E.; Robb, M. A.; Cheeseman, J. R.; Scalmani, G.; Barone, V.; Mennucci, B.; Petersson, G. A.; Nakatsuji, H.; Caricato, M.; Li, X.; Hratchian, H. P.; Izmaylov, A. F.; Bloino, J.; Zheng, G.; Sonnenberg, J. L.; Hada, M.; Ehara, M.; Toyota, K.; Fukuda, R.; Hasegawa, J.; Ishida, M.; Nakajima, T.; Honda, Y.; Kitao, O.; Nakai, H.; Vreven, T.; Montgomery, J. A., Jr.; Peralta, J. E.; Ogliaro, F.; Bearpark, M.; Heyd, J. J.; Brothers, E.; Kudin, K. N.; Staroverov, V. N.; Keith, T.; Kobayashi, R.; Normand, J.; Raghavachari, K.; Rendell, A.; Burant, J. C.; Iyengar, S. S.; Tomasi, J.; Cossi, M.; Rega, N.; Millam, J. M.; Klene, M.; Knox, J. E.; Cross, J. B.; Bakken, V.; Adamo, C.; Jaramillo, J.; Gomperts, R.; Stratmann, R. E.; Yazyev, O.; Austin, A. J.; Cammi, R.; Pomelli, C.; Ochterski, J. W.; Martin, R. L.; Morokuma, K.; Zakrzewski, V. G.; Voth, G. A.; Salvador, P.; Dannenberg, J. J.; Dapprich, S.; Daniels, A. D.; Farkas, O.; Foresman, J. B.; Ortiz, J. V.; Cioslowski, J.; Fox, D. J. *Gaussian 09*, Revision D. 01; Gaussian Inc.: Wallingford, CT, 2013.

(18) Chai, J.-D.; Head-Gordon, M. Systematic Optimization of Long-Range Corrected Hybrid Density Functionals. *J. Chem. Phys.* **2008**, *128*, 084106.

(19) Chai, J.-D.; Head-Gordon, M. Long-Range Corrected Hybrid Density Functionals with Damped Atom−Atom Dispersion Corrections. *Phys. Chem. Chem. Phys.* **2008**, *10*, 6615−6620.

(20) Hehre, W. J.; Ditchfield, R.; Pople, J. A. Self-Consistent Molecular Orbital Methods. XII. Further Extensions of Gaussian-Type Basis Sets for Use in Molecular Orbital Studies of Organic Molecules. *J. Chem. Phys.* **1972**, *56*, 2257−2261.

(21) Hariharan, P. C.; Pople, J. A. The Influence of Polarization Functions on Molecular Orbital Hydrogenation Energies. *Theor. Chim. Acta* **1973**, *28*, 213−222.

(22) Dolg, M.; Stoll, H.; Savin, A.; Preuss, H. Energy-Adjusted Pseudopotentials for the Rare Earth Elements. *Theor. Chim. Acta* **1989**, *75*, 173−194.

(23) Marenich, A. V.; Cramer, C. J.; Truhlar, D. G. Universal Solvation Model Based on Solute Electron Density and on a

Continuum Model of the Solvent Defined by the Bulk Dielectric Constant and Atomic Surface Tensions. *J. Phys. Chem. B* **2009**, *113*, 6378−6396.
(24) Regueiro-Figueroa, M.; Esteban-Gómez, D.; de Blas, A.; Rodríguez-Blas, T.; Platas-Iglesias, C. Understanding Stability Trends along the Lanthanide Series. *Chem. - Eur. J.* **2014**, *20*, 3974−3981.
(25) Martell, A. E.; Hancock, R. D. *Metal Complexes in Aqueous Solutions*; Plenum Press: New York, 1996.
(26) Peters, J. A.; Djanashvili, K.; Geraldes, C. F. G. C.; Platas-Iglesias, C. The Chemical Consequences of the Gradual Decrease of the Ionic Radius along the Ln-Series. *Coord. Chem. Rev.* **2020**, *406*, 213146.
(27) Gans, P.; O'Sullivan, B. GLEE, a New Computer Program for Glass Electrode Calibration. *Talanta* **2000**, *51*, 33−37.
(28) Gans, P.; Sabatini, A.; Vacca, A. Investigation of Equilibria in Solution. Determination of Equilibrium Constants with the HYPERQUAD Suite of Programs. *Talanta* **1996**, *43*, 1739−1753.
(29) Gans, P.; Sabatini, A.; Vacca, A. Determination of Equilibrium Constants from Spectrophometric Data Obtained from Solutions of Known pH: the Program pHab. *Ann. Chim.* **1999**, *89*, 45−49.
(30) Thiele, N. A.; Brown, V.; Kelly, J. M.; Amor-Coarasa, A.; Jermilova, U.; MacMillan, S. N.; Nikolopoulou, A.; Ponnala, S.; Ramogida, C. F.; Robertson, A. K. H.; Rodríguez-Rodríguez, C.; Schaffer, P.; Williams, C., Jr.; Babich, J. W.; Radchenko, V.; Wilson, J. J. An Eighteen-Membered Macrocyclic Ligand for Actinium-225 Targeted Alpha Therapy. *Angew. Chem., Int. Ed.* **2017**, *56*, 14712−14717.
(31) Aluicio-Sarduy, E.; Thiele, N. A.; Martin, K. E.; Vaughn, B. A.; Devaraj, J.; Olson, A. P.; Barnhart, T. E.; Wilson, J. J.; Boros, E.; Engle, J. W. Establishing Radiolanthanum Chemistry for Targeted Nuclear Medicine Applications. *Chem. - Eur. J.* **2020**, *26*, 1238−1242.
(32) Reissig, F.; Bauer, D.; Ullrich, M.; Kreller, M.; Pietzsch, J.; Mamat, C.; Kopka, K.; Pietzsch, H.-J.; Walther, M. Recent Insights in Barium-131 as a Diagnostic Match for Radium-223: Cyclotron Production, Separation, Radiolabeling, and Imaging. *Pharmaceuticals* **2020**, *13*, 272.
(33) Abou, D. S.; Thiele, N. A.; Gutsche, N. T.; Villmer, A.; Zhang, H.; Woods, J. J.; Baidoo, K. E.; Escorcia, F. E.; Wilson, J. J.; Thorek, D. L. J. Towards the Stable Chelation of Radium for Biomedical Applications with an 18-Membered Macrocyclic Ligand. *Chem. Sci.* **2021**, *12*, 3733−3742.
(34) Fiszbein, D. J.; Brown, V.; Thiele, N. A.; Woods, J. J.; Wharton, L.; MacMillan, S. N.; Radchenko, V.; Ramogida, C. F.; Wilson, J. J. Tuning the Kinetic Inertness of Bi^{3+} Complexes: The Impact of Donor Atoms on Diaza-18-Crown-6 Ligands as Chelators for ^{213}Bi Targeted Alpha Therapy. *Inorg. Chem.* **2021**, *60*, 9199−9211.
(35) Stasiuk, G. J.; Long, N. J. The Ubiquitous DOTA and its Derivatives: the Impact of 1,4,7,10-Tetraazacyclododecane-1,4,7,10-tetraacetic Acid on Biomedical Imaging. *Chem. Commun.* **2013**, *49*, 2732−2746.
(36) Cacheris, W. P.; Nickle, S. K.; Sherry, A. D. Thermodynamic study of Lanthanide Complexes of 1,4,7-Triazacyclononane-*N*,*N*′,*N*″-triacetic Acid and 1,4,7,10-Tetraazacyclododecane-*N*,*N*′,*N*″,*N*‴-tetraacetic Acid. *Inorg. Chem.* **1987**, *26*, 958−960.
(37) Roca-Sabio, A.; Mato-Iglesias, M.; Esteban-Gómez, D.; Tóth, É.; de Blas, A.; Platas-Iglesias, C.; Rodríguez-Blas, T. Macrocyclic Receptor Exhibiting Unprecedented Selectivity for Light Lanthanides. *J. Am. Chem. Soc.* **2009**, *131*, 3331−3341.
(38) Thiele, N. A.; MacMillan, S. N.; Wilson, J. J. Rapid Dissolution of $BaSO_4$ by Macropa, an 18-Membered Macrocycle with High Affinity for Ba^{2+}. *J. Am. Chem. Soc.* **2018**, *140*, 17071−17078.
(39) Hu, A.; Keresztes, I.; MacMillan, S. N.; Yang, Y.; Ding, E.; Zipfel, W. R.; DiStasio, R. A., Jr.; Babich, J. W.; Wilson, J. J. Oxyaapa: A Picolinate-Based Ligand with Five Oxygen Donors that Strongly Chelates Lanthanides. *Inorg. Chem.* **2020**, *59*, 5116−5132.
(40) Grimes, T. S.; Nash, K. L. Acid Dissociation Constants and Rare Earth Stability Constants for DTPA. *J. Solution Chem.* **2014**, *43*, 298−313.
(41) Moeller, T.; Thompson, L. C. Observations on the Rare Earths—LXXV: The Stabilities of Diethylenetriaminepentaacetic Acid Chelates. *J. Inorg. Nucl. Chem.* **1962**, *24*, 499−510.
(42) Pniok, M.; Kubíček, V.; Havlíčková, J.; Kotek, J.; Sabatie-Gogová, A.; Plutnar, J.; Huclier-Markai, S.; Hermann, P. Thermodynamic and Kinetic Study of Scandium(III) Complexes of DTPA and DOTA: A Step Toward Scandium Radiopharmaceuticals. *Chem. - Eur. J.* **2014**, *20*, 7944−7955.
(43) Karle, I. L. Hydrogen Bonds in Molecular Assemblies of Natural, Synthetic and 'Designer' Peptides. *J. Mol. Struct.* **1999**, *474*, 103−112.
(44) Toth, E.; Brucher, E.; Lazar, I.; Toth, I. Kinetics of Formation and Dissociation of Lanthanide(III)−DOTA Complexes. *Inorg. Chem.* **1994**, *33*, 4070−4076.
(45) van Leeuwen, H. P.; Town, R. M.; Buffle, J. Impact of Ligand Protonation on Eigen-Type Metal Complexation Kinetics in Aqueous Systems. *J. Phys. Chem. A* **2007**, *111*, 2115−2121.
(46) van Leeuwen, H. P.; Town, R. M. Outer-Sphere and Inner-Sphere Ligand Protonation in Metal Complexation Kinetics: The Lability of EDTA Complexes. *Environ. Sci. Technol.* **2009**, *43*, 88−93.
(47) Deblonde, G. J.-P.; Zavarin, M.; Kersting, A. B. The Coordination Properties and Ionic Radius of Actinium: A 120-Year-Old Enigma. *Coord. Chem. Rev.* **2021**, *446*, 214130.
(48) Pommé, S.; Marouli, M.; Suliman, G.; Dikmen, H.; Van Ammel, R.; Jobbágy, V.; Dirican, A.; Stroh, H.; Paepen, J.; Bruchertseifer, F.; Apostolidis, C.; Morgenstern, A. Measurement of the ^{225}Ac Half-Life. *Appl. Radiat. Isot.* **2012**, *70*, 2608−2614.
(49) Geerlings, M. W.; Kaspersen, F. M.; Apostolidis, C.; van der Hout, R. The Feasibility of ^{225}Ac as a Source of α-Particles in Radioimmunotherapy. *Nucl. Med. Commun.* **1993**, *14*, 121−125.
(50) Thiele, N. A.; Wilson, J. J. Actinium-225 for Targeted α Therapy: Coordination Chemistry and Current Chelation Approaches. *Cancer Biother. Radiopharm.* **2018**, *33*, 336−348.
(51) Eychenne, R.; Chérel, M.; Haddad, F.; Guérard, F.; Gestin, J.-F. Overview of the Most Promising Radionuclides for Targeted Alpha Therapy: The "Hopeful Eight". *Pharmaceutics* **2021**, *13*, 906.
(52) McDevitt, M. R.; Ma, D.; Simon, J.; Frank, R. K.; Scheinberg, D. A. Design and Synthesis of ^{225}Ac Radioimmunopharmaceuticals. *Appl. Radiat. Isot.* **2002**, *57*, 841−847.
(53) Kadassery, K. J.; King, A. P.; Fayn, S.; Baidoo, K. E.; MacMillan, S. N.; Escorcia, F. E.; Wilson, J. J. H_2BZmacropa-NCS: A Bifunctional Chelator for Actinium-225 Targeted Alpha Therapy. *Bioconjugate Chem.* **2022**, *33*, 1222−1231.

https://doi.org/10.1021/acs.inorgchem.2c01998
Inorg. Chem. 2022, 61, 12847−12855